Chinese Chemical Letters 34 (2023) 107255

Contents lists available at ScienceDirect

Chinese Chemical Letters

journal homepage: www.elsevier.com/locate/cclet

Highly emissive coordination polymer derived from tetraphenylethylene-tetrazole chromophore: Synthesis, characterization and piezochromic luminescent behavior

Xu Han[a], Jialin Tong[b], Guanyu Ding[a], Chunyi Sun[b], Xinlong Wang[b], Zhongmin Su[a,*], Jing Sun[a], Li-Li Wen[a,*], Guo-Gang Shan[b,*]

[a] School of Chemical and Environmental Engineering, Changchun University of Science and Technology, Changchun 130022, China
[b] National & Local United Engineering Laboratory for Power Batteries, Key Laboratory of Polyoxometalate Science of Ministry of Education, Department of Chemistry, Northeast Normal University, Changchun 130024, China

ARTICLE INFO

Article history:
Received 9 January 2022
Revised 9 February 2022
Accepted 21 February 2022
Available online 24 February 2022

Keywords:
Coordination polymer
Piezochromic luminescence
Aggregation-induced emission
Stimulus-response
Sensing

ABSTRACT

Solid-state materials that exhibit pressure stimulus-response characteristics in a manner of emission signal, known as piezochromic luminescence (PCL), demonstrate great potential in photoelectric devices. The weakened luminescence and insignificant color change in the aggregation state, however, hampers their practical applications. Herein, a highly emissive coordination polymer, $[Zn_2(H_4TTPE)(H_2O)_4]\cdot H_2O$ (**CUST-805**), is successfully constructed by employing an AIE-active chromophore as the building block. The structural characterization and photophysical properties are systematically studied. Owing to intrinsic twisted conformation and AIE feature of tetraphenylethylene-tetrazole ligand, **CUST-805** achieves the visible and reversible PCL from blue to green switched by different external stimuli. The transformation between crystalline and amorphous states is proved to be the origin of present PCL behavior. Moreover, on basis of electron and energy transfer quenching mechanism, the highly selective and sensitive sensor based on **CUST-805** is realized, showing the low detection limit of 0.29 ppm towards 2,4,6-trinitrophenol.

The coordination polymers (CPs) have received tremendous attention in the industrial and academic communities since the pioneering work reported by Yaghi in the middle 90s [1–4]. CPs usually consist of metal nodes and organic linkers *via* covalent bonds assembled into one-, two- and three-dimensional (1D-3D) crystalline networks [5–7]. In particular, their inherent advantages of versatile structures, tunable pore sizes, and exposed active sites [8,9], make CPs promising candidates for luminescence [10,11], sensing [12–14], catalysis [15,16], and adsorption fields [17,18]. The development of luminescent CPs has become a hot topic in the past decade [19,20]. However, the traditional aggregation-caused quenching (ACQ) effect of employed organic linkers always leads to poor luminous efficiencies of the resulting CPs, limiting their application in the optical field [21]. Significant advances have been made in improving the emission efficiency, however, the challenges remain.

Recently, a fascinating photophysical phenomenon, aggregation-induced emission (AIE), has attracted considerable attention, in which AIE-active molecules exhibit weak or no emission in isolation but strong luminescence in solid-state or when confined by surrounding microenvironment [22–24]. Such promising characteristics of AIE luminophores open a new avenue for the development of solid-state luminescent materials with high efficiency as well as desired functionality [25,26]. Tetraphenylethylene (TPE), the most explored luminophore core, is commonly used as the building block to construct diverse AIE materials including pure organic small molecules and organic-inorganic hybrid [27]. Dincă and colleagues have devoted enormous efforts to deciphering the intrinsic mechanism of TPE-based MOF materials and demonstrated their outstanding potential in turn-on sensors [28]. Zhou's group utilized an extended TPE-based carboxylate linker with zirconium salt to give rise to highly fluorescent Zr-based MOF, whose emission color is reversibly switched between blue and green upon different external stimulations [29]. Restricted molecular motions in the rigid matrix and switchable topologies under pressure endow CP as a new family of piezochromic luminescent materials. Recent reviews have summarized the processes and breakthroughs on AIE

* Corresponding authors.
E-mail addresses: zmsu@nenu.edu.cn (Z. Su), wll@cust.edu.cn (L.-L. Wen), shangg187@nenu.edu.cn (G.-G. Shan).

https://doi.org/10.1016/j.cclet.2022.02.060
1001-8417/

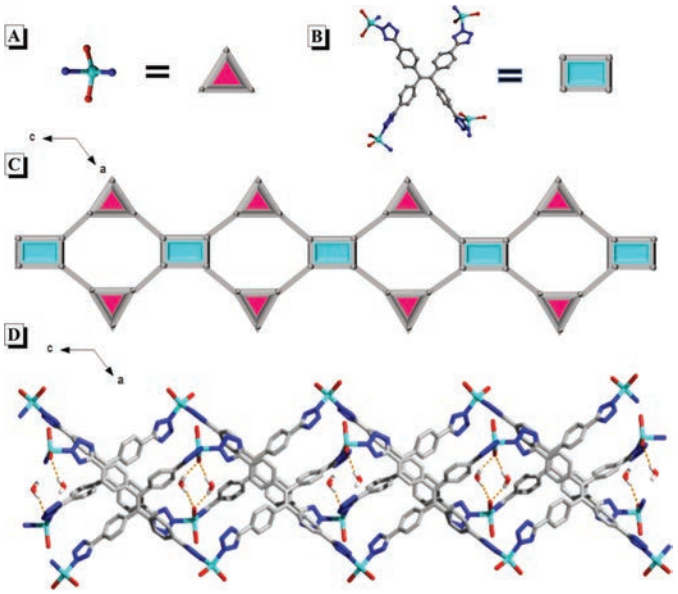

Fig. 1. The structure of **CUST-805**. (A) Zn cluster and (B) organic ligand viewed as a pair of nodes lines, as well as (C) simplified of the self-assembled 1D chain along the b direction. (D) Perspective view of the H_2O cluster linking two chains. Hydrogen bonds are depicted as yellow striped bonds. Color modes: Zn, turquoise, N, blue, O red, C gray-25%, H white.

chromophores-based materials [30–33]. However, the development of stimulus-responsive CPs with strong luminescence and good reversibility is still in its infancy [34].

Taking the characteristic of iconic TPE moiety as well as excellent coordination ability of tetrazole together, herein, a high emissive CP material named **CUST-805**, is designed and synthesized accordingly, as shown in Fig. 1. **CUST-805** can be easily prepared by metal clusters Zn^{2+} ions and tetrakis[4-(1*H*-tetrazol-5-yl)phenyl]ethylene (H_4TTPE) under the solvothermal condition. The characterizations and photophysical properties were systematically investigated. As expected, the resulting CP not only exhibits bright emission with the photoluminescence quantum yield (PLQY) of 46.4% but also has piezochromic behavior with the significant and reversible color change and enhanced PLQY once the mechanical grinding is applied. Inspired by the bright emission of **CUST-805** in the aggregated state, a highly selective and sensitive explosive probe toward 2,4,6-trinitrophenol (TNP) is also achieved.

White crystals of **CUST-805** were obtained by the solvothermal reaction of H_4TTPE and Zn^{2+} ions with a molar ratio of 1:5 in percent of C_2H_5OH and $NH_3{\cdot}H_2O$ mixture. The synthetic details can be found in supporting information (for experimental section) and the visible images of **CUST-805** crystals are depicted in Fig. S1 (Supporting information). Single-crystal X-ray diffraction analysis indicates that **CUST-805** crystallizes in a monoclinic space group of *C2/c* and adopts a 1D ribbon chain structure. The asymmetric unit of **CUST-805** is composed of two crystallographically independent Zn^{II} ions, four water molecules, one organic $TTPE^{4-}$, and a free water molecule (Fig. S2 in Supporting information). The two types of Zn^{II} metal center adopt a distorted triangular pyramid $\{ZnN_2O_2\}$ geometry, which is defined by two nitrogen atoms from $TTPE^{4-}$ ligand and two oxygen atoms from two molecules (Fig. 1A), while each $TTPE^{4-}$ ligand links four Zn nodes (Fig. 1B) are further self-assembled to extend into a 1D ribbon chain along the *b* axis as exhibited in Fig. 1C. The Zn-N bond distances vary from 2.4038(9) Å to 2.4618(11) Å and the Zn-O bond lengths range from 2.236(2) Å to 2.297(3) Å. In the crystal state of **CUST-805**, abundant interactions of O-H···O stacking could be observed along with the b direction and thus giving rise to 2D layer, as illustrated in Fig. 1D and Fig. S3 (Supporting information). Additionally, 3D supramolecular architecture is formed *via* intermolecular interactions of O-H···O and π-π stacking (3.55 Å) between neighboring 2D planes (Fig. S4 in Supporting information).

The phase purity of synthesized **CUST-805** is examined by powder X-ray diffraction (PXRD) pattern. The diffraction spectrum of the experimental product is consistent with the theoretical simulation data as exhibited in Fig. S5A (Supporting information). In addition, **CUST-805** shows relatively good thermal stability, as supported by the thermogravimetric analysis data (TGA) (Fig. S5B in Supporting information). The main functional groups' absorption bands of **CUST-805** are tested by the fourier transform infrared (FT-IR) spectrum (Fig. S5C in Supporting information), which reveals that the wide peak appeared at 3334 cm^{-1} represents the quantity of the O–H groups of the water molecules and the bands at 1400-1650 cm^{-1} perhaps are related to the tensile vibrational of aromatic CN. The bands at 800-1300 cm^{-1} area may be interrelated to the H_4TTPE tetrazole ligands. Furthermore, the chemical stability of **CUST-805** is explored in Figs. S5 and S6 (Supporting information). There is no doubt that the excellent stability of **CUST-805**, providing a nice foundation for further application.

To study the emission behavior of **CUST-805**, the emission spectra in different states are measured. As illustrated in Figs. 2A and B, the as-prepared white crystals of **CUST-805** emit bright blue fluorescence with an emission maximum of 464 nm under UV light. Interestingly, the emission color of powders changes from blue to green upon grinding with a pestle, which can be easily observed by the naked eyes. The ground sample hereafter denoted as **CUST-805G** exhibits a red-shifted wavelength with a peak of 520 nm compared with that of freshly prepared **CUST-805**. In addition to the bathochromic shifted spectrum, the photoluminescent quantum yield is improved from 46.4% for **CUST-805** to 84.9% for **CUST-805G** (Fig. S7 in Supporting information). The tight packing as well as the restricted rotations of the aromatic rings may be attributed to the above phenomenon [35–37]. The excited-state lifetimes (τ) experiments are then determined to further understand intrinsic photophysical processes. The decay lifetimes of **CUST-805** and **CUST-805G** in the solid-state are 2.98 ns and 6.26 ns, respectively, as demonstrated in Fig. S8 (Supporting information). The radiative rate constants ($k_f = \Phi/\tau$) for **CUST-805** is thus 1.6×10^8 s^{-1}, which is close to 1.4×10^8 s^{-1} for **CUST-805G**. In contrast, the non-radiative rate constant [$k_{nr} = (1\text{-}\Phi)/\tau$] is greatly decreased from 1.8×10^8 for **CUST-805** to 2.4×10^7 s^{-1} for **CUST-805G**. Moreover, the solid absorption spectra of **CUST-805** and **CUST-805G** are investigated and the corresponding data are illustrated in Fig. S9 (Supporting information), and the TGA data of **CUST-805G** is shown in Fig. S10 (Supporting information). The original white crystals change into faint yellow with the board and red-shifted absorption bands for **CUST-805G** in comparison with that observed for **CUST-805,** which is in good agreement with the photographic images shown in Fig. 2A. To prove that the present piezochromic process is reversible, we conduct grinding and heating tests. The emission color, as well as the daylight color of **CUST-805G,** can revert to the original color upon annealing the ground sample in a mixture of ammonia and ethanol, resulting in a heated sample named **CUST-805H**. Further grinding **CUST-805H**, the blue-emitting powders change into green-emitting again. Such color switching between blue and green are thus repeated four times without any fatigue, suggesting good reversibility (Fig. S11 in Supporting information). The sensitivity of **CUST-805** response to pressure stimuli in a reversible dynamic luminescence shift, which can be better visualized by the CIE diagram (Fig. S12 in Supporting information).

To gain insight into the piezochromic luminescence property, X-ray diffraction (XRD) patterns of **CUST-805**, **CUST-805G** and **CUST-805H** in solid-states are studied. The pristine crystal of **CUST-805** exhibit numerous intense and sharp reflection peaks that

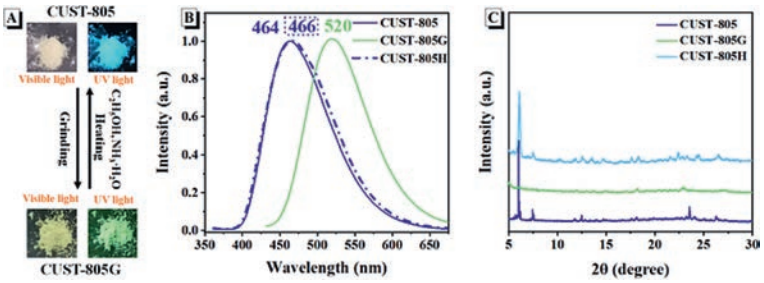

Fig. 2. (A) The visual and fluorescence color change from **CUST-805** to **CUST-805G** powder samples. (B) Fluorescent spectra of **CUST-805** (solid line, blue), **CUST-805G** (solid line, green), and **CUST-805H** (dotted line, blue) at room temperature. (C) PXRD patterns of **CUST-805** (blue), **CUST-805G** (green), and **CUST-805H** (navy blue).

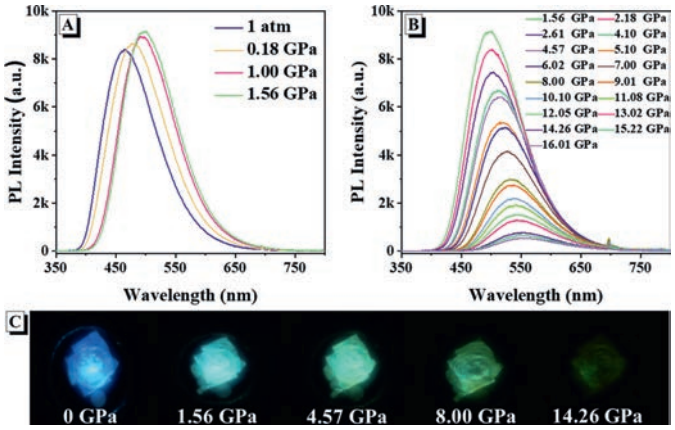

Fig. 3. (A, B) Emission spectra and (C) fluorescent images of **CUST-805** under pressure from 0 GPa to 14.26 GPa.

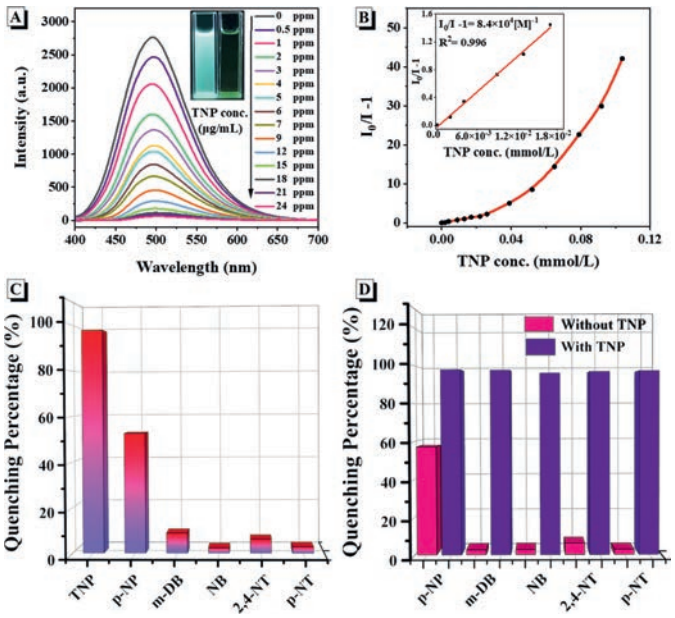

Fig. 4. (A) Fluorescent spectrum of **CUST-805** in DMF containing different amounts of TNP. (B) Corresponding S-V plots of TNP. Inset: the fitting curves of the linear S-V plots for TNP at low concentrations (20 μmol/L). (C) Quenching percentage obtained of different analytes (24 ppm). (D) Column diagrams of the relative fluorescence intensity of **CUST-805** with different analytes at 496 nm. pink bars represent the addition of various analytes in DMF and violet bars represent the subsequent addition of TNP (24 ppm) to the above solutions (**CUST-805** + analytes + TNP).

are indicative of a well-defined crystal structure. The diffraction curves of **CUST-805G**, however, exhibit a wide and weak peak, indicating that the amorphous states are formed. Some sharp diffraction peaks appeared again for annealed sample **CUST-805H**, as shown in Fig. 2C. These results demonstrate that the heating can convert amorphous ground samples to the crystalline states possibly through molecular repacking, and hence the reversible piezochromic luminescence behavior. Piezochromic mechanism of **CUST-805** may be related to morphology change from the stretched and loose crystalline state to the more planar and tighter amorphous phase [38].

The behavior of piezochromic effect is further verified by hydrostatic pressure instead of irregular grinding. Since both twisted skeleton and variable spaces exit in **CUST-805**, the drastic framework deformation would happen, if the mechanical force is imposed. We studied the luminescent change of **CUST-805** under varied high-pressures in the diamond anvil cell experiments. With pressure increasing from 1 atm to 1.56 GPa, **CUST-805** crystal displays red-shifted emission from blue (462 nm) to green (500 nm) accompanied with enhanced emission intensity. Meanwhile, the emission peak reaches its maximum intensity at 1.56 GPa. With further compression to 14.26 GPa, the red-shifted emission is observed from 500 nm to 550 nm, along with a monotonic decrease in intensity (Figs. 3A and B). Furthermore, after 1.56 GPa, there is a linear correlation between the emission logarithm of the relative intensity, $\ln(I_0/I_i)$ and pressures (Fig. S13 in Supporting information). The fluorescent images of **CUST-805** under different pressures are displayed in Fig. 3C. **CUST-805** exhibits a red-shift transition, which may be due to its conformational flexibility and the facile modification of weak intermolecular interactions under high pressure [38,39].

As studied above, 1D CPs possess more accessible active sites and afford rapid mass transport and charge transfer, endowing them enhanced performance in sensing applications [40,41]. Considering nitroaromatic explosives are a serious threat to human health and national homeland security, sensitive and selective detection of nitroaromatic explosives is of great significance [42–44]. After the addition of 24 ppm TNP, the fluorescence intensity of **CUST-805** is reduced to only 2.3% of the original one (Fig. 4A). In contrast, other nitroaromatic explosives, such as 4-nitrophenol (*p*-NP), 1,3-dinitrobenzene (*m*-DB), nitrobenzene (NB), 2,4-dinitrotoluene (2,4-NT) and *p*-nitrotoluene (*p*-NT), have little or no effect on the emission of **CUST-805** (Fig. S14 in Supporting information). The results demonstrate that **CUST-805** has high selectivity for TNP among a variety of nitroaromatic explosives (Fig. 4C). The fluorescence quenching efficiency can be quantified using Stern-Volmer equation and the K_{SV} is estimated to be 8.40×10^4 mmol/L on basis of S-V plot (Fig. 4B), which is comparable or even better than those of the previously reported CP sensors for TNP detection (Table S5 in Supporting information). Meanwhile, the TNP sensor based on **CUST-805** also shows a low detection limit of 0.29 ppm.

These phenomena encouraged us to explore the ability of **CUST-805** to detect TNP under the interference of other potential nitroaromatic explosives. A slight fluorescence quenching occurred upon the addition of 24 ppm others explosives. In contrast, once adding 24 ppm TNP into the above mixture behaved a significant and rapid emission quenching of **CUST-805** is observed (Fig. 4D). The assay outstanding data for TNP reveal that **CUST-805** is an excellent sensor for the sensitive and selective detection of TNP.

To comprehend the high selectivity origin of **CUST-805** for TNP, the mechanism of quenching is investigated. TNP has the stabilized lowest unoccupied molecular orbital (LUMO) energy levels among all studied nitroaromatic explosives (Fig. S15 and Table S6 in Supporting information), and the LUMO of H_4TTPE has higher energy compared to the LUMO of the TNP. Efficient electrons transfer thus can easily occur from the LUMO of **CUST-805** to TNP, thus resulting in fluorescence quenching of **CUST-805.** To check whether the energy transfer quenching mechanism is involved in the sensing, the UV-vis absorption spectra of nitroaromatic explosives are recorded [45,46]. As shown in Fig. S16 (Supporting information), there is the obvious overlaps absorption spectrum of TNP and emission spectrum of **CUST-805**, indicating the accessible fluorescence resonance energy transfer between them, which further quenches emission of **CUST-805**. Therefore, it is speculated that the synergy of electron and energy transfer quenching mechanisms may be responsible for the high selectivity and sensitivity of **CUST-805** for the detection of TNP.

In conclusion, we have employed AIE-active tetrakis[4-(1*H*-tetrazol-5-yl)phenyl]ethylene and zinc(II) ion as a ligand and metal node, respectively, to successfully construct a highly emissive CP. The resulting CP, **CUST-805**, not only exhibits bright light with QY of 46.4% but also efficient PCL behavior with the significant color change from blue to green accomplished with an enhanced QY of 84.9%. The green-emitting color caused by grinding can recover to the original one by heating treatment, and such switching can be repeated many times without fatigue. The experiment result suggests that the transformation from crystalline to amorphous states is attributed to the present PCL behavior triggered by grinding. Moreover, a linear correlation between emission intensity and hydrostatic pressure can be established. Moreover, a highly selective and sensitive sensor towards TNP is also achieved. The excellent performance of **CUST-805** makes it a promising candidate for use as pressure sensors, explosive detection as well as other optical application, and the results obtained herein would provide a feasible way to construct multifunctional coordination polymers with highly emissive and controllable external stimulus-response behavior in the future.

Declaration of competing interest

The authors declare that they have no known competing financial interests or personal relationships that could have appeared to influence the work reported in this paper.

Acknowledgments

We are thankful for the financial support from the National Natural Science Foundation of China (No. 22175033), Science and Technology Development Plan of Jilin Province (Nos. YDZJ202101ZYTS063, 2021050822RQ).

Supplementary materials

Supplementary material associated with this article can be found, in the online version, at doi:10.1016/j.cclet.2022.02.060.

References

[1] G. Givaja, P. Amo-Ochoa, C. J.Gómez-García, F. Zamora, Chem. Soc. Rev. 41 (2012) 115–147.
[2] H.R. Moon, D.W. Lim, M.P. Suh, Chem. Soc. Rev. 42 (2013) 1807–1824.
[3] M. Yoon, K. Suh, S. Natarajan, K. Kim, Angew. Chem. Int. Ed. 52 (2013) 2688–2700.
[4] J.P. Zhang, Y.B. Zhang, J.B. Lin, X.M. Chen, Chem. Rev. 112 (2012) 1001–1033.
[5] W.G. Lu, Z.W. Wei, Z.Y. Gu, et al., Chem. Soc. Rev. 43 (2014) 5561–5593.
[6] Y.H. Wen, Q. Liu, S.D. Su, et al., Nanoscale 12 (2020) 12767–12772.
[7] S.L. Li, T.X. Xiao, C. Lin, L.Y. Wang, Chem. Soc. Rev. 41 (2012) 5950–5968.
[8] T. Luo, G.T. Nash, Z.W. Xu, et al., J. Am. Chem. Soc. 143 (2021) 13519–13524.
[9] M. Safaei, M.M. Foroughi, N. Ebrahimpoor, et al., Trends Analyt. Chem. 118 (2019) 401–404 25.
[10] X.G. Yang, D.P. Yan, Chem. Sci. 7 (2016) 4519–4526.
[11] H.L. Jiang, Q. Xu, Chem. Comm. 47 (2011) 3351–3370.
[12] S. Wang, Q.Y. Wang, X. Feng, B. Wang, L. Yang, Adv. Mater. 29 (2017) 1701898–1701914.
[13] K. Miyata, Y. Konno, T. Nakanishi, et al., Angew. Chem. Int. Ed. 52 (2013) 6413–6416.
[14] P. Mahata, S.K. Mondal, D.K. Singha, P. Majee, Dalton Trans. 46 (2017) 301–328.
[15] Z.H. Yan, M.H. Du, J.X. Liu, et al., Nat. Commun. 9 (2018) 3353–3361.
[16] J. Wang, A.S. Cherevan, C. Hannecart, et al., Appl. Catal. B 283 (2021) 119626–119637.
[17] N.C. Burtch, H. Jasuja, K.S. Walton, Chem. Rev. 114 (2014) 10575–10612.
[18] Y.F. Gu, J.J. Zheng, K. Otake, et al., Angew. Chem. Int. Ed. 60 (2021) 11688–11694.
[19] J.Q. Liu, Z.D. Luo, Y. Pan, et al., Coord. Chem. Rev. 406 (2020) 213145–213190.
[20] O. Guillou, C. Daiguebonne, G. Calvez, K. Bernot, Acc. Chem. Res. 49 (2016) 844–856.
[21] Y.H. Wei, H.Y. Dong, C. Wei, et al., Adv. Mater. 28 (2016) 7424–7429.
[22] M.M. Kang, Z.J. Zhang, N. Song, et al., Aggregate 1 (2020) 80–106.
[23] Y.N. Hong, J.W.Y. Lam, B.Z. Tang, Chem. Soc. Rev. 40 (2011) 5361–5388.
[24] W.L. Shang, X.F. Zhu, T.L. Liang, et al., Angew. Chem. Int. Ed. 59 (2020) 12811–12816.
[25] Q.H. Gong, Z.C. Hu, B.J. Deibert, et al., J. Am. Chem. Soc. 136 (2014) 16724–16727.
[26] J.J. Pang, R.H. Du, X. Lian, et al., Chin. Chem. Lett. 32 (2021) 2443–2447.
[27] H.Q. Yin, X.Y. Wang, X.B. Yin, J. Am. Chem. Soc. 141 (2019) 15166–15173.
[28] N.B. Shustova, B.D. McCarthy, M. Dincă, J. Am. Chem. Soc. 133 (2011) 20126–20129.
[29] Q. Zhang, J. Su, D.W. Feng, et al., J. Am. Chem. Soc. 137 (2015) 10064–10067.
[30] Y. Zhang, S. Xie, Z.B. Zeng, B.Z. Tang, Matter 3 (2020) 1862–1892.
[31] Y.Z. Liu, X.Y. Guan, Q.R. Fang, Aggregate 2 (2021) 34–48.
[32] L.Y. Zhu, B. Zhu, J. Luo, B. Liu, ACS Mater. Lett. 3 (2021) 77–89.
[33] L. Ma, X. Feng, S. Wang, B. Wang, Mater. Chem. Front. 1 (2017) 2474–2486.
[34] Y.J. Kong, Z.P. Yan, S. Li, et al., Angew. Chem. Int. Ed. 59 (2020) 5336–5340.
[35] O. Toma, M. Allain, F. Meinardi, et al., Angew. Chem. Int. Ed. 128 (2016) 8130–8134.
[36] Z.W. Wei, C.X. Chen, S.P. Zheng, et al., Inorg. Chem. 55 (2016) 7311–7313.
[37] M. Andrzejewski, A. Katrusiak, J. Phys. Chem. Lett. 8 (2017) 279–284.
[38] C.X. Chen, Z.W. Wei, Y.N. Fan, et al., Chem 4 (2018) 2658–2669.
[39] Z.Q. Yao, J. Xu, B. Zou, et al., Angew. Chem. Int. Ed. 58 (2019) 5614–5618.
[40] D. Voiry, H.S. Shin, K.P. Loh, M. Chhowalla, Nat. Rev. Chem. 2 (2018) 1–17.
[41] Z.W. Jiang, Y.C. Zou, T.T. Zhao, et al., Angew. Chem. Int. Ed. 132 (2020) 3326–3332.
[42] Y.X. Guo, X. Feng, T.Y. Han, et al., J. Am. Chem. Soc. 136 (2014) 15485–15488.
[43] L.H. Shi, N. Li, D.M. Wang, et al., Trends Analyt. Chem. 134 (2021) 116131–116150.
[44] M.E. Germain, M.J. Knapp, Chem. Soc. Rev. 38 (2009) 2543–2555.
[45] Y. Peng, A.J. Zhang, M. Dong, Y.W. Wang, Chem. Comm. 47 (2011) 4505–4507.
[46] X.G. Liu, C.L. Tao, H.Q. Yu, et al., J. Mater. Chem. C 6 (2018) 2983–2988.